A methane sink in the Central American high elevation páramo: Topographic, soil moisture and vegetation effects

Leanne L. Chai[a], Guillermo Hernandez-Ramirez[a,*], David S. Hik[b], Isabel C. Barrio[c], Carol M. Frost[a], Cristina Chinchilla Soto[d], Germain Esquivel-Hernández[e]

[a] Department of Renewable Resources, University of Alberta, Edmonton, Canada
[b] Department of Biological Sciences, Simon Fraser University, Burnaby, Canada
[c] Department of Natural Resources and Environmental Sciences, Agricultural University of Iceland, Árleyni 22, IS-112 Reykjavík, Iceland
[d] Environmental Pollution Research Center, Universidad de Costa Rica, San Jose, Costa Rica
[e] Stable Isotope Research Group, School of Chemistry, Universidad Nacional Costa Rica, 86-3000 Heredia, Costa Rica

ARTICLE INFO

ABSTRACT

Methane (CH_4) is a strong greenhouse gas with a global warming potential 23 times larger than that of carbon dioxide. Characterizing ecosystems as either sources or sinks for methane and their magnitudes informs on biosphere contributions to the global CH_4 budget and to warming of the atmosphere. We quantified methane fluxes for the first time in a neotropical alpine páramo (Valle de Los Conejos, Chirripó Massif, Costa Rica) and examined the relationships of these fluxes with topography, soil moisture and vegetation, during the transition from dry to rainy season. Using closed chambers and laser spectroscopy, we measured soil CH_4 and CO_2 fluxes across a field site encompassing: a grassy plain as well as a plain, a gentle slope and a plateau dominated by a dwarf bamboo (*Chusquea subtessellata* Hitchcock). We found that the páramo landscape acts as a sink for CH_4 $[-53.1 \pm 29.6$ (mean $\pm$ SE) µg C m^{-2} hr^{-1}]. Of the four field areas, the grassy plain was on average the strongest CH_4 sink, likely because this soil profile had no drainage restrictions and was well aerated. By contrast, in the slope and plateau, a heavily-consolidated subsurface layer was shown to perch water, increasing surface soil moisture and limiting CH_4 uptake. Conversely, in certain parts of the plain, where *Chusquea* grew vigorously in discrete, tall patches, we found intense CH_4 uptake beneath these patches. Within the *Chusquea* plain, these hot spots of CH_4 uptake localized under the tall *Chusquea* had double the uptake rates than outside these patches, with even greater uptake than the average in the grassy plain. Our results show that CH_4 uptake in the páramo is driven by moisture interacting with impeding soil layers, vegetation and topography.

1. Introduction

The atmospheric concentration of methane (CH_4), a potent greenhouse gas, is in part regulated by soils, as they both produce and consume CH_4 through microbial processes (Chen et al., 2013). The resulting net CH_4 flux is primarily governed by abiotic factors such as soil moisture, porosity, aeration, gas exchange, substrate availability, temperature, and the presence of water table (Chen et al., 2013; Serrano-Silva et al., 2014; Hofmann et al., 2016; Meier et al., 2016; Kou et al., 2017; Sjogersten et al., 2018). Earlier studies have documented that fluctuations of soil moisture display one of the strongest controls on CH_4 uptake (Jang et al., 2006; Torn and Harte, 1996; Wei et al., 2015; He et al., 2014) as moisture transiently regulates aeration and the proportion of aerobic pores (favoring CH_4 consumption) to anaerobic

microsites (leading to CH_4 production) within the soil (Chen et al., 2013; Hofmann et al., 2016). Vegetation type and associated peat organic matter properties may also play a role in determining small-scale spatial variation in methane production (Girkin et al., 2019).

Characterizing the intensity of sources or sinks of methane across a broad range of terrestrial ecosystems worldwide will inform on their contributions to the global CH_4 budget. As most recent attention has been on deciphering greenhouse gas exchange in managed ecosystems (Kim et al., 2013; Lin et al., 2017), several natural ecosystems still remain critically understudied with respect to the direction and magnitude of their CH_4 fluxes. For instance, no data are currently available in the literature for the neotropical páramo ecosystems. The páramo is a high-elevation mountain ecosystem between the tree ecotone (~3000 m above sea level, masl) and the nival line (~4500 masl)

geographically distributed in Central and South America between 11°N and 8°S (Schneidt et al., 1996; Buytaert et al., 2006a). This neotropical alpine environment is inherently unique, characterized by topographical heterogeneity, rich natural biodiversity and water provisioning services (Hofstede et al., 2003; Buytaert et al., 2006a; Célleri et al., 2010). Earlier reports have shown that alpine ecosystems around the world can vary from net methane uptake (Koch et al., 2007; Kato et al., 2011; Wei et al., 2015), to nearly null flux (Imer et al., 2013) and even net emission (Teh et al., 2014). New research efforts can address the variability and uncertainty of methane exchange in alpine regions and the specific paucity of flux information for the páramo.

The role of vegetation in ecosystem CH_4 exchange is just beginning to be understood (Hofmann et al., 2016; Meier et al., 2016; Kou et al., 2017; Brachmann, 2019). Vegetation indirectly impacts the soil physical environment by changing soil moisture and gas diffusivity; therefore, vegetation and soils interactively regulate CH_4 fluxes (Meier et al., 2016). For example, decreasing soil moisture with increasing vegetation coverage was found to generate a strong methane sink in a temperate alpine ecosystem (Brachmann, 2019). Likewise, vegetation type affects CH_4 fluxes through further indirect effects on the soil environment (Meier et al., 2016); in non-saturated landscapes, roots can mediate the formation of soil structure enabling pathways for gas diffusion and aeration status (Chen et al., 2011), and hence, creating favorable conditions for methanotrophy (Serrano-Silva et al., 2014; Kou et al., 2017; Girkin et al., 2019). In addition to these indirect physical impacts on soil CH_4 exchange, plant growth supports soil biological activity by regulating the microclimate and contributing inputs to the soil organic matter cycling. The type and abundance of vegetation can affect CH_4 and CO_2 fluxes through their litter, root and exudate production, leading to accretion or depletion of organic matter pools in soils. Not only do the additional organic carbon and associated nutrients act as a substrate to support the soil microbial community and activity, but they also improve soil aggregation and structure, leading to increases in porosity, and hence, indirectly also aiding gas diffusion (Tanthachoon et al., 2008; Meier et al., 2016). Such indirect vegetation effects can be examined by means of quantifying the surface fluxes of CO_2 as reported by McKnight et al. (2017) in an Ecuadorian páramo with contrasting land use histories. Although the stimulating effects of available heat and moisture on soil fluxes of CO_2 have been well documented for other biomes (Hernandez-Ramirez et al., 2011, Curtin et al., 2012), these controlling relationships are only beginning to be explored in páramo ecosystems (McKnight et al., 2017).

Our objectives were to (i) determine the source or sink potential of CH_4 in the Central American páramo during the transition from dry to rainy season (from 7 to 11 April 2018), and to (ii) examine changes in soil surface CH_4 fluxes across field variations in topography, soils and vegetation, which were also hypothesized to be underlying driving factors for these fluxes. We anticipated that topography would indirectly impact CH_4 fluxes by redistributing water in the landscape creating zones of higher and lower soil moisture, and hence lower and higher exchange of gases, respectively. Soil type dictates the distribution of texture and structure both across the landscape and vertically in the soil profile, which also strongly relate to water availability, aeration and gas diffusion. Likewise, vegetation indirectly affects soil moisture through uptake, evaporation and structure formation through root growth. Moreover, we also examined at a much finer spatial scale how CH_4 fluxes are influenced by the dominant plant species in the páramo, the dwarf bamboo (*Chusquea subtessellata* Hitchcock) and by differences in soil moisture. In addition, to document the overall soil biological activity (including soil and root respirations), we evaluated the surface CO_2 fluxes although our main focus remained on CH_4.

2. Materials and methods

2.1. Site description

The study site was located in the Valle de Los Conejos, Chirripó National Park, Costa Rica (latitude 9° 28′ 1.98″ N; longitude 83° 29′ 23.19″ W; mean elevation of 3480 masl). This remote alpine valley is part of the high Talamanca mountain range. There is evidence of late Quaternary glaciation; the ecosystem is classified as páramo (Schneidt et al., 1996; Orvis and Horn, 2000; Kappelle and Horn, 2016). The Páramo ecosystem covers about 35,000 km^2 surface along Central and South America (Buytaert et al., 2006b), comprising approximately 2% of the land area (Beniston, 2000; Kappelle and Horn, 2016). The Central American páramo is confined to the highlands of Costa Rica and Panama with terrain elevations ranging from 3000 to 3820 masl. In Costa Rica, the total surface of páramo is 15,205 ha (~0.3% of the country), and with most of the páramo located within the boundaries of the Chirripó National Park (est. in 1975) with a surface of 10,395 Ha (Kappelle and Horn, 2016).

The mean annual temperature is 9.8 °C and mean annual precipitation is 1884 mm year^{-1}, with 86% of the rainfall occurring between May and November (Chirripó National Park Weather Station located near Crestones Base Camp at an elevation of 3440 masl and with records from 2000 to 2013; Supplementary Fig. 1). Shifts in tropospheric wind circulation during the year produce two rainfall maxima: one in May and one in October (Durán-Quesada et al., 2017; Magaña et al., 1999).

Our study site with an approximate area of 7500 m^2 (Fig. 1B) was dominated by the nearly ubiquitous and endemic dwarf bamboo *Chusquea subtessellata*, and also by the grass *Festuca dolichophylla* (Schneidt et al., 1996; Kappelle and Horn, 2016). As this site exhibited strong stratification by distinctive terrain-vegetation zones, we divided our site into four sub-areas according to field topographic positions, landforms and dominant vegetation types: (i) a plain dominated by grass vegetation (grassy plain), (ii) a plain dominated by tall *Chusquea* (tall *Chusquea* plain), (iii) a slope dominated by short *Chusquea* (short *Chusquea* slope), and (iv) a plateau dominated by short *Chusquea* (short *Chusquea* plateau) (Fig. 1). This study site encompassing these four adjacent field sub-areas represents effectively contrasting portions of the typical páramo ecosystem in Central America as it includes the two main plant community types (i.e., páramo ecosystem type dominated by the bamboo *C. subtessellata* or by the grass *F. dolichophylla*) as well as the two most common landforms (plain and slope). Furthermore, based on the geomorphological and vegetation variations across these four adjacent sub-areas, the collective field gradient across our study site was treated and examined as a soil toposequence typically found throughout the páramo region, and which likely develops from widespread soil forming factors such as similar parent materials, topography and climate.

With the aim of characterizing the *Chusquea* vegetation present at the study site, we measured *Chusquea* plants (n = 100) and categorized them into two characteristic groups: short and tall. The tall *Chusquea* (common in one of the plain sub-areas) grew in distinctively vigorous patches or clumps, with a mean maximum canopy height of 1.66 ± 0.06 m and radii mean at the ground level of 0.67 ± 0.10 m (n = 33), while the short *Chusquea* plants (commonly found across the slope and plateau sub-areas) were more scattered and smaller, with maximum height of 0.57 ± 0.04 m, and radii mean of 0.12 ± 0.02 m (n = 67). Furthermore, the separation distance between short *Chusquea* vegetation in the slope sub-area was typically 3 m, while openings between patches of tall *Chusquea* within the plain sub-area were much wider (4 to 7 m separation distance).

Five soil profiles were excavated in selected field locations along the toposequence in our study site to document the underlying pedogenic attributes and their variations (Fig. 1). The location and elevation of each soil profile was recorded using repeated measurements with a
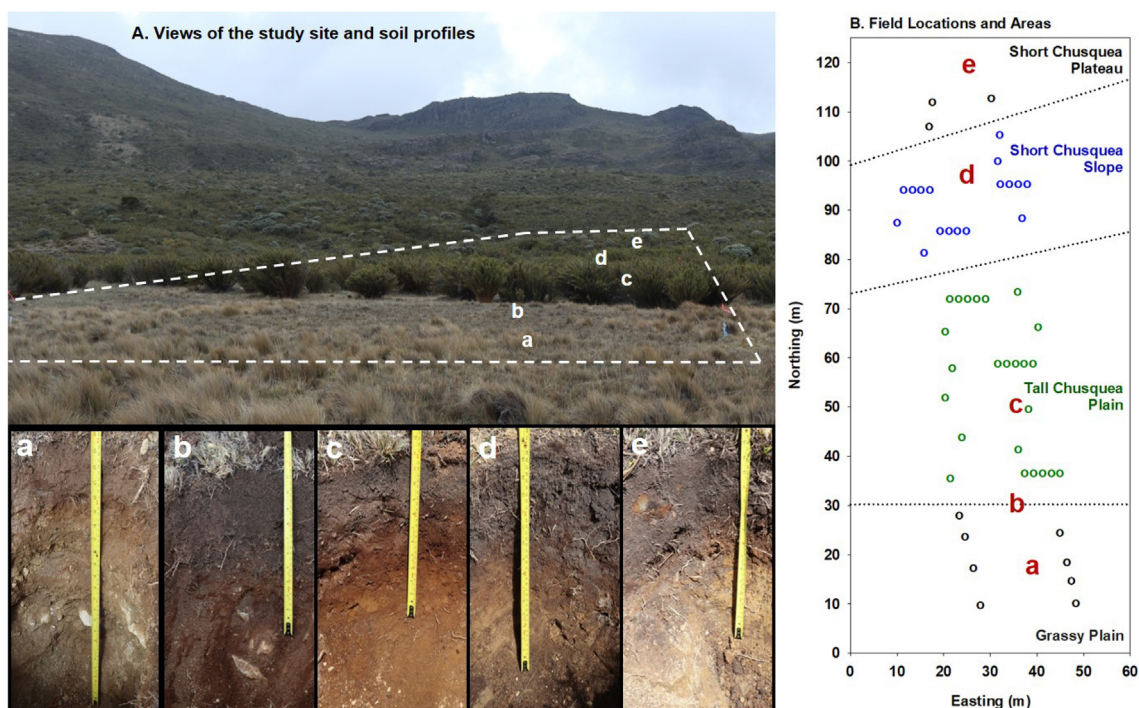
Fig. 1. Conejos study site in Chirripó National Park, Costa Rica. (A) General boundary of study site and locations of five soil profiles (a–e). Soil profile attributes and classification along the field site can be found in Table 1. (B) A total of 52 chamber bases were installed for repeated flux measurements including six nested locations to investigate smaller scale variations associated to patches of *Chusquea subtesellata*. The individual positions of the chambers are indicated by circles; as noted, four sub-areas of the study site were further delineated according to field topographic positions and dominant vegetation type; reference point 0, 0 corresponds to latitude 9° 28′ 1.98″ N and longitude 83° 29′ 23.19″ W.

portable GPS receiver (Garmin™ eTrex 20). Following the Canadian System of Soil Classification (Soil Classification Working Group, 1998), the detailed profile descriptions showed that the soil in the grassy plain was a well-drained Orthic Humic Regosol (a soil in an early development stage; the approximately-correspondent FAO and USDA soil classifications are Regosol and Entisols, respectively), transitioning into a slightly more developed Orthic Sombric Brunisol (FAO and USDA correspond to Dystric Cambisol and Humbric Dystrochrepts) as the tall *Chusquea* became the dominant vegetation in the plain. Soils on both the slope and plateau sub-areas were Rego Humic Gleysols (FAO and USDA correspond to Umbric Gleysol and Humaquepts) with imperfect drainage (Table 1). Soil samples were collected from each soil horizon and profile, transported with icepacks for preservation, passed through a 2 mm sieve, and analyzed for chemical composition (Table 1). Soil pH and electrical conductivity were quantified in soil:water ratio of 10:25. Electrical conductivity resulted in 0.1 dS m^{-1} across all soil horizons and profiles. Concentrations of organic carbon and nitrogen were measured via dry combustion. Phosphorus and potassium concentrations followed the modified Olsen method at pH 8.5, soil:extractant ratio of 1:10 and colorimetry method. Ammonium was quantified in a 2 M KCl extraction followed by colorimetry. Exchangeable ions were extracted with 1 M KCl (1:10) followed by atomic absorption spectrometry.

2.2. Surface flux measurements

A custom-made, non-steady state, flow-through chamber method was used to measure the change in gas concentration with time in order to calculate the gaseous flux. The chamber had two components: a chamber base (5 cm total height) and a chamber lid (12 cm inner height), both made of cylindrical polyvinyl chloride with inner diameter of 10 cm. The chamber lid was equipped with a gasket and a rubber band for sealing the edges of the lid with the chamber base during flux measurement. A vent tubing in the chamber lid enabled

equilibration of the chamber headspace with the outside atmospheric pressure. The external surfaces of the chamber were covered with reflective tape to prevent any potential overheating from solar radiation. The cylindrical chamber bases were installed perpendicular to the ground surface about 24 h before the beginning of our flux measurements. Upon installation of the chamber bases, we measured an average height of 1.8 ± 0.1 cm above the ground, and they were kept in place for the duration of the field measurements.

Soil flux measurements were conducted twice a day (in the morning within 8:30 AM to 12:00 noon, and again in the afternoon within 12:30 PM to 4:00 PM) during five consecutive days from 7 to 11 April 2018. This measurement period coincided with the beginning of the rainy season in the Chirripó Massif (Fig. 2). During this measurement period, the available air temperature records showed no consistent diel (24-hour cycle) fluctuations (Supplementary Fig. 2). These weather conditions recorded at Crestones served the purpose of demonstrating the typical meteorological conditions prevailing at the Chirripó páramo during the 2018 drier months and the onset of the rainy season when our study took place (Esquivel-Hernández et al., 2019).

A total of 52 chamber locations were distributed across our study site to collect measurements along the soil toposequence and vegetation gradient encompassing all four field sub-areas (Fig. 1B). With the aim of examining any influence of proximity to the dominant páramo vegetation on the soil fluxes, certain groups of chambers were established along several short (1.44 or 1.92 m) transects placed radially from the center of the *Chusquea* plants. The tall *Chusquea* plain sub-area had three sets of these groups, each with five chambers. The central chamber location was installed at the center of the *Chusquea* patch, the next chamber location typically corresponded to near the edge of the *Chusquea* patch, while the other three chamber locations were equally spaced moving away from the *Chusquea* patch. Likewise, the short *Chusquea* slope sub-area had three sets of these groups in a similar arrangement, but each group with only four chambers because of the reduced open spaces among neighboring *Chusquea* plants in the slope

Table 1

Soil profile attributes and classification at the Valle de Los Conejos, Chirripó National Park, Costa Rica. The soil profile locations along the toposequence in the study site are shown in Fig. 1. Soil description followed the Canadian System of Soil Classification (Soil Classification Working Group, 1998). Further methodology details are available in the Site Description section. ECEC stands for effective cation exchange capacity.

| Profile Location	Field Sub-area Denomination	Elevation (at the soil surface) masl	Dominant Plant Species	Soil Classification	Drainage Class	Depth to lithic contact cm	Horizon Designation	Horizon Depth cm	Texture (tactile)	Carbon % (w/w)	Nitrogen % (w/w)	C:N Ratio	Ammonium mg N Kg^{-1}	Phosphorus mg P L^{-1}	pH	ECEC cmol$_+$ L^{-1}	Acid Saturation %
a	Grassy Plain	3479	*Festuca dolichophylla*	Orthic Humic Regosol	Well	55	Ah	0–10	Loam	13.00	1.05	12.4	11.0	2	4.9	3.85	76
							Bm	10–14	Loam	5.00	0.49	10.2	6.8	1	5.2	1.49	56
							C1	14–35	Clay Loam	4.1	0.14	9.0	4.1	3	5.5	1.04	42
							C2	35–55	Sand	0.59	0.07	8.4	7.8	6	5.6	1.47	42
b	Transition between Grassy Plain and Tall Chusquea Plain	3480	*F. dolichophylla and Chusquea subtessellata*	Orthic Sombric Brunisol	Well	31	Ah	0–13	Loam	14.39	1.36	10.6	8.7	3	4.7	4.21	75
							Bm	13–31	Sandy Loam	5.58	0.45	12.4	6.1	2	5.0	3.01	78
c	Tall Chusquea Plain	3481	*C. subtessellata*	Orthic Sombric Brunisol	Well	37	Ah	0–11	Loam	13.40	1.13	11.9	15.8	2	4.8	3.89	66
							Bm	11–24	Loam	9.96	0.76	13.1	6.1	1	4.9	4.16	83
							C	24–37	Loamy Sand	1.78	0.13	13.7	8.0	3	4.5	2.25	71
d	Short Chusquea Slope	3483	*C. subtessellata*	Rego Humic Gleysol	Imperfect	52	LFH	2–0	–	–	–	–	–	–	–	–	–
							Ah	0–13	Loam	22.92	1.87	12.3	12.0	6	4.4	5.78	76
							Bm	13–23	Loam	15.14	1.24	12.2	9.4	4	4.6	5.67	81
							Cg	23–52	Silty Clay Loam	3.31	0.26	12.7	6.7	2	5.0	2.79	78
e	Short Chusquea Plateau	3487	*C. subtessellata*	Rego Humic Gleysol	Imperfect	45	LFH	3–0	–	–	–	–	–	–	–	–	–
							Ah	0–13	Loam	18.36	1.59	11.5	14.3	3	4.5	4.46	80
							Bm	13–20	Loam	11.62	0.96	12.1	15.3	2	4.8	4.52	83
							Cg	20–45	Loam-Clay Loam	3.45	0.26	13.3	11.1	1	4.8	3.17	79
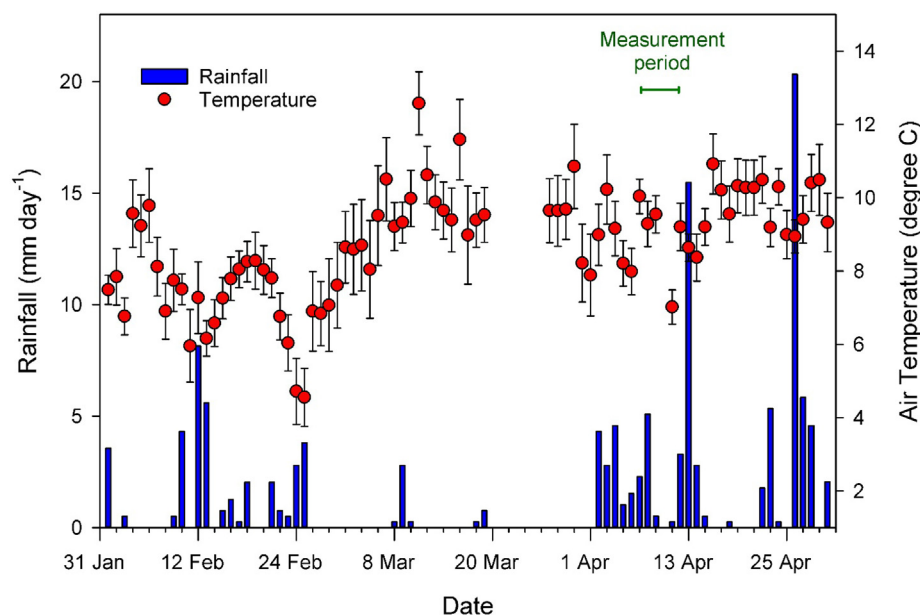
Fig. 2. Daily cumulative rainfall and mean air temperature assembled from readings every 30 min at a weather station near Crestones Base Camp, Chirripó National Park (09° 27′ N, 83° 30′ W; elevation 3440 masl; located ~2 Km from the Conejos study site) encompassing January to April 2018. Weather station was installed and data recorded by Universidad Nacional Costa Rica as described in Esquivel-Hernández et al. (2018). Error bars are standard errors of the data available for each day.

sub-area as aforementioned. Within these transects, the distance between neighboring chamber locations was 48 cm. The arrangement of these grouped chambers was intended to capture any flux variability as a function of proximity to *Chusquea* (Fig. 3). The tall *Chusquea* plain sub-area also had another 9 chamber bases installed individually and distributed in the grassy openings between *Chusquea* patches (Fig. 1B). Likewise, the short *Chusquea* slope sub-area also had another 5 chamber bases installed individually. Overall, there were 8 chamber locations in the grassy plain sub-area, 24 in the tall *Chusquea* plain (15 + 9), 17 in the short *Chusquea* slope (12 + 5), and 3 in the short *Chusquea* plateau.

With the intention of quantifying only the soil surface gaseous fluxes, all chamber bases (10 cm diameter) were installed in non-vegetated locations (on bare ground either between *Chusquea* stems or between grass clumps, with no growing plants within the chamber). Using repeated measurements with a portable GPS receiver (Garmin™ eTrex 20) at each chamber location, the average terrain elevations of the flux-chamber locations within each of the four field sub-areas were 3479, 3479, 3482 and 3485 masl for the grassy plain, tall *Chusquea* plain, short *Chusquea* slope and short *Chusquea* plateau, respectively.

When collecting gaseous flux measurements, the chamber lid was placed on top of the chamber base and secured with a peripheral rubber band for sealing the headspace. The chamber was closed for 3 mins while the gas concentrations were continuously measured *in situ*. Subsequently, the chamber lid was removed and allowed to flush and equilibrate with ambient air for at least one minute before beginning the next flux measurement.

The gas concentrations were measured using a Picarro GasScouter G4301, which is a portable cavity ring-down spectroscopy (CRDS) laser analyzer equipped with an internal vacuum pump (Picarro, Inc, Santa Clara, CA, USA) (Brachmann, 2019). The recirculation method involved using a pair of teflon tubings (one-fourth inch O.D.) to pump air at a constant flow rate (i.e., 0.81 standard liters per minute) from the chamber headspace through the optical CRDS analytical cell and back to the chamber headspace. The mixing ratios of the analytes (i.e., CH_4, CO_2 and H_2O) were averaged and recorded every 1.25 s. While the focus of the flux measurements was on CH_4, both CO_2 and water vapor data were also recorded. The CO_2 flux data provided an indication of biological activity, and water vapor concentration was used to automatically correct all concentration data to dry air basis. The analytical detection limits of instrumentation for the CH_4 and CO_2 concentrations were found to be 0.68 ppb and 0.130 ppm, respectively, based on three times the standard deviation as derived from 77 min of our continuous

concentration measurements using zero-air standard gas in a laboratory room.

The CH_4 and CO_2 fluxes of each chamber were determined using the modified ideal gas law as follows:

$$Flux = S \times P \times V \times A^{-1} \times R^{-1} \times T^{-1} \times 12 \quad gCmol^{-1} \tag{1}$$

where flux is the gaseous rate of the analyte (µg C m^{-2} hr^{-1}); S is the slope of the linear regression derived from the time series of analyte concentration with time (µL L^{-1} hr^{-1}); P is the ambient pressure (Pa); V is the headspace volume for each of the chambers (L); A is the ground surface area within the chamber (m^2); R is the gas constant (Pa L K^{-1} mol^{-1}) and T is the ambient air temperature (K). The multiplication by 12 g mol^{-1} is necessary to express the fluxes in terms of carbon mass in CH_4 and CO_2. The derived regression coefficients extracted through linear fitting were screened against the following criteria: the p-value of the regression coefficient must be lower than 0.05 and coefficients of determination must be higher than 0.95. Flux measurements that did not meet these requirements were excluded from further data analyses. Out of the potential total of 520 methane flux measurements during our study, 472 flux values were retained in the dataset and 48 were excluded.

2.3. Ancillary field measurements and weather data

Measurements of soil moisture, soil temperature, air temperature, infrared surface temperature, and ambient pressure were taken close to each chamber base location for each of the flux measurements. Volumetric soil moisture (% v/v) and soil temperature (°C) were measured in the 0–6 cm surface soil layer using a portable digital soil probe (Stevens® Hydra-Probe), air temperature (°C) was measured with a shielded digital thermometer (Traceable®, VWR part no. 61220–601) probe, surface temperature (°C) was measured using an infrared radiometer (Apogee® MI-230), and ambient air pressure (Pa) was measured with a handheld sensor (Testo® 511). Ambient air temperature and pressure were used as inputs to inform Eq. (1). Meteorological conditions for 2018 were recorded using a weather station installed by Universidad Nacional Costa Rica (as described in Esquivel-Hernández et al., 2018) at the Crestones Base Camp (elevation of 3440 masl) about 2 km west from the study site.
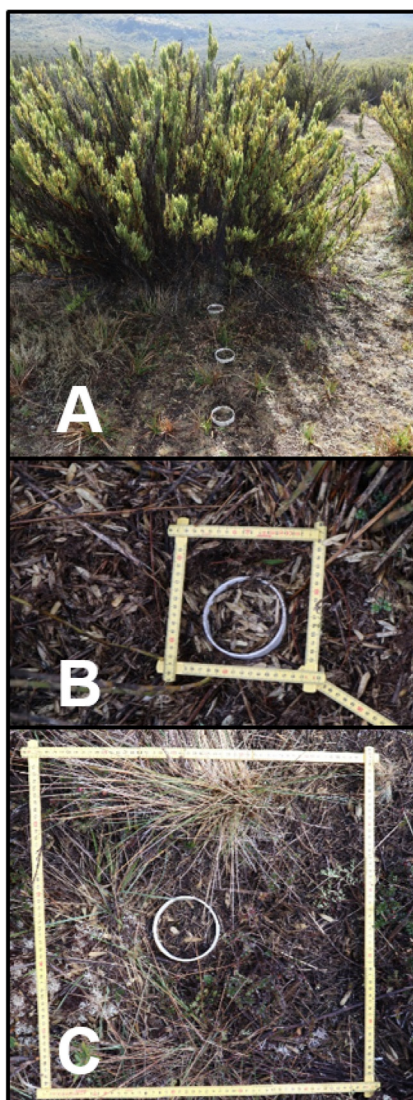
Fig. 3. Views of flux chamber locations arranged in short-distance transects within the field sub-area denominated: tall *Chusquea* plain. (A) Chamber bases were installed in the ground radiating out from the center of a vigorous *Chusquea* patch into adjacent natural openings. (B) View of a chamber base located at the center of a *Chusquea* patch; a 15 cm × 15 cm frame was included for spatial reference. (C) Close view of a chamber base located about 1.2 m away from *Chusquea* vegetation (reference frame is 50 cm × 50 cm).

2.4. Statistics

We used repeated measurement analyses of variance (ANOVA) followed by Tukey tests to assess differences in soil moisture between the four field sub-areas. Where the data normality assumption was not fulfilled (e.g., CH_4 and CO_2 fluxes), we performed Kruskal-Wallis ANOVA on ranks followed by Dunn tests. We also assessed the differences in methane fluxes at a smaller spatial scale for chambers at different positions relative to the *Chusquea* patches using Kruskal-Wallis ANOVA on ranks and Dunn tests, given the non-normal distribution of the CH_4 flux data. Additionally, we fitted linear or polynomial regression lines to evaluate the relationship between methane fluxes and soil moisture. Analyses were performed using R software (ver. 3.3.1) and SigmaStat (ver. 4.0) with an alpha critical value of 0.05.
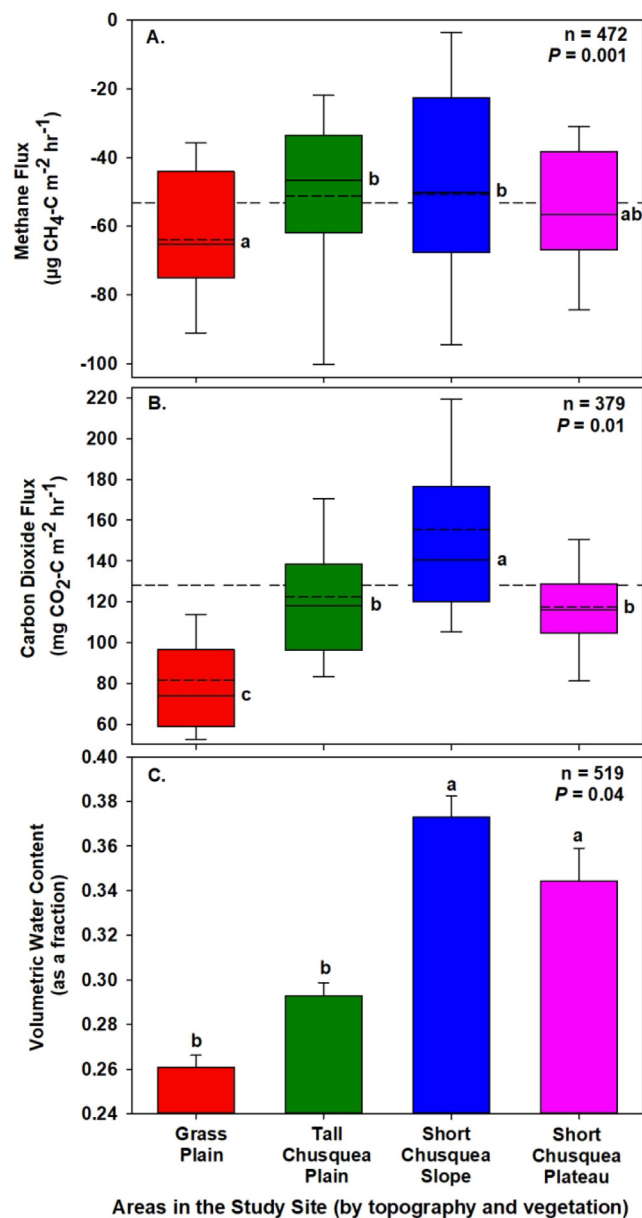

Fig. 4. (A) Methane and (B) carbon dioxide fluxes, and (C) soil volumetric water content in the 0–6 cm surface soil layer comparing the four terrain-vegetation sub-areas in our study site. Lower case letters indicate the comparison grouping. The reference horizontal dash lines in panels A and B correspond to the overall flux mean in these datasets. Box plot representation in panels A and B: whiskers are the 10th and 90th percentiles, boundaries of the boxes are 25th and 75th percentiles, continuous horizontal lines within the boxes are the medians, and discontinuous horizontal lines are the means. Error bars in panel C are standard errors. As shown in Fig. 1B, there were 8 chamber locations in the grassy plain sub-area, 24 in the tall *Chusquea* plain, 17 in the short *Chusquea* slope, and 3 in the short *Chusquea* plateau. The number of methane flux observations for each field sub-area (as shown in panel A) are = grassy plain: 65, tall *Chusquea* plain: 209, short *Chusquea* slope: 170, and short *Chusquea* plateau: 28. The number of carbon dioxide flux observations for each field sub-area (as shown in panel B) are = grassy plain: 54, tall *Chusquea* plain: 167, short *Chusquea* slope: 136, and short *Chusquea* plateau: 22.

3. Results

3.1. Surface gaseous fluxes

The average CH_4 flux measured for the entire dataset was -53.1 ± 29.6 (mean ± SE) µg CH_4-C m^{-2} hr^{-1} (Fig. 4A). When

evaluating these fluxes by field sub-areas, the largest uptake of CH_4 occurred in the grassy plain (-63.9 µg CH_4-C m^{-2} hr^{-1}), and this CH_4 influx was significantly different from the tall *Chusquea* plain (-51.2 µg CH_4-C m^{-2} hr^{-1}) and the short *Chusquea* slope (-50.8 µg CH_4-C m^{-2} hr^{-1}), while the intermediate fluxes in the short *Chusquea* plateau (-56.6 µg CH_4-C m^{-2} hr^{-1}) did not show significant differences from the other field sub-areas (Fig. 4A).

We identified a significant spatial effect of the distance away from the center of *Chusquea* vegetation on the measured CH_4 fluxes. Strikingly, we found that the methane uptake was typically high beneath the center of the tall *Chusquea* patches (-101 µg CH_4-C m^{-2} hr^{-1}) compared to outside these patches (-52 µg CH_4-C m^{-2} hr^{-1}) within the *Chusquea* plain sub-area (Fig. 7A). In contrast, this spatial difference was not observed at all with the short *Chusquea* vegetation within the slope field sub-area (Fig. 7B).

The surface CO_2 fluxes averaged 128.0 mg CO_2-C m^{-2} hr^{-1}, and statistical differences were found between a lower flux in the grassy plain (81.5 mg CO_2-C m^{-2} hr^{-1}), a relatively high flux at tall *Chusquea* plain (122.2 mg CO_2-C m^{-2} hr^{-1}) and the even higher efflux at the short *Chusquea* slope (155.3 mg CO_2-C m^{-2} hr^{-1}) (Fig. 4B). It can be noted that, on average, the grassy plain exhibited both the strongest CH_4 uptake and the lowest CO_2 emission.

3.2. Soil moisture and temperature

Our study site showed an ample variation in soil moisture with observations ranging widely from 6 to 68% (Figs. 5A and 6). With the
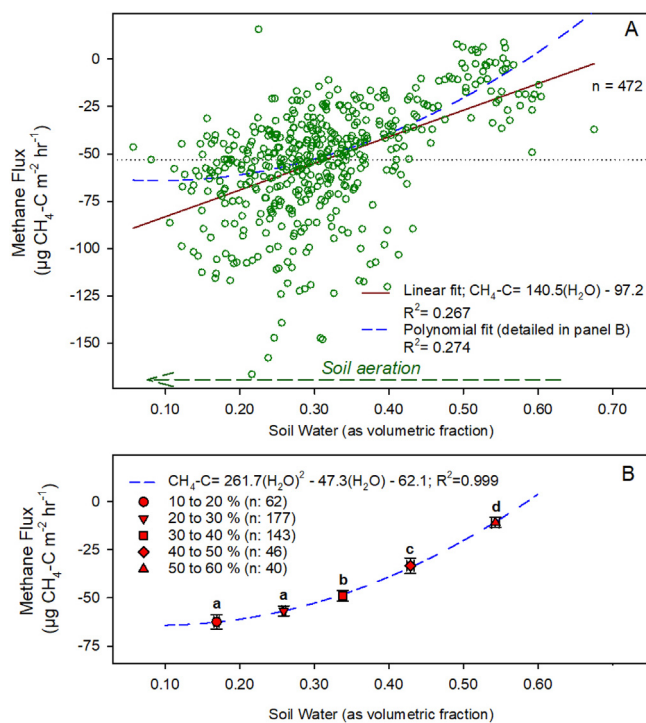

Fig. 5. Surface methane fluxes as a function of soil volumetric water content in the 0–6 cm surface soil layer. (A) All individual flux-moisture measurements; the polynomial fitting is the same as in panel A (included here for reference); linear fitting (conducted for exploratory purposes) derived from ordinary least square regression ($P < 0.001$); for reference, the horizontal dotted line corresponds to the overall flux mean in this entire dataset. (B) Individual flux measurements were classified into five classes of soil volumetric water content (from 10 to 60% as indicated in the panel legend); bidirectional error bars are standard errors; a polynomial fitting described the noticeable curvilinear response; lower case letters (a-d) indicate the flux comparison and grouping across the five moisture classes ($P < 0.001$; Kruskal-Wallis ANOVA on ranks and Dunn test).

aim of further exploring the CH_4 flux-moisture relationship, we integrated the individual flux-moisture observations by binning this dataset into five classes (Fig. 5B). The resulting five pairs of central estimates effectively reduced the noise in both variables (in part as an effect of the bidirectional binning of the large sample sizes), and a slightly convex pattern emerged where CH_4 uptake in general rose with relatively drier soils (Fig. 5B).

When comparing moisture across the four field sub-areas, our repeated field measurements clearly revealed that soil water content at the surface layer was significantly higher at the short *Chusquea* slope (37% v/v) and plateau (34%) compared with the tall *Chusquea* plain (29%) and the open grassy plain (26%) (Fig. 4C). It is noticeable that soils under the short *Chusquea* were significantly wetter than in the tall *Chusquea* plain although their CH_4 fluxes were similar (Fig. 4A and 4C).

Additionally, while assessing the spatial effect of distance away from the *Chusquea* vegetation, significantly drier soil conditions were found in the farthest locations outside of both the tall *Chusquea* (Fig. 7C) and the short *Chusquea* vegetation (Fig. 7D). Soil water content was typically 8–9% higher directly beneath the *Chusquea* plants than in the soils under the surrounding grass-dominated areas (Fig. 7C and 7D). Likewise, upon quantifying air temperature, ground surface temperature (infrared) and soil temperature at various distances away from the center of the *Chusquea* vegetation, it became evident that ground surface temperature was much more responsive to the presence of vegetation than air or soil temperatures. While mean changes in air or soil temperatures across the various distances were only about 2 °C, ground surface temperature revealed significant differences, with a much reduced temperature directly at the center of the tall *Chusquea* patches than at the chamber locations outside the shadow of this vegetation, with a difference of 8.5 °C (13.5 vs. 22 °C, respectively; Fig. 7G). Noticeably, the short *Chusquea* vegetation also showed a tendency toward this same directional effect although it was not significant (Fig. 7H).

3.3. Soil profile description

Upon excavating and sampling by horizons five soil profiles along the study site, chemical analyses revealed that soil organic carbon and nitrogen concentrations in the A horizons were consistently enriched (i.e., 16.4 ± 1.5% C and 1.40 ± 0.12% N; Table 1) which suggests high storage of organic matter and also to some extent soil fertility to sustain plant growth; however, laboratory results indicated that these A soil horizons exhibited acid reaction (pH: 4.7, acid saturation: 75%) and were depleted in nutrients such as phosphorus (Table 1).

A clear change in texture was observed vertically across the soil horizons, but only in the soil profiles located in the slope and plateau field sub-areas dominated by short *Chusquea*. While the shallower soil horizons (A and B) registered relatively light texture (i.e., Loam – pedogenically derived from wind-blown loess parent material), the texture became heavier in the deeper C horizons (with more clay contents such as Silty Clay Loam – pedogenically associated with dense glacial till parent material deposited and compressed during the most recent glaciation) which also exhibited mosaic-color features of soil gleyzation (Cg) associated with reduced movement of water (Table 1). By contrast, the plain areas (either dominated by grass or tall *Chusquea*) did not display these soil morphologic features and profile patterns at all.

4. Discussion

4.1. Fluxes of CH_4 and CO_2 along the toposequence

The predominantly negative CH_4 fluxes found during the beginning of the rainy season suggest that the neotropical páramo landscape acts as a sink for methane (i.e., negative fluxes; Fig. 4A). This is in general agreement with earlier studies measuring methane flux elsewhere in
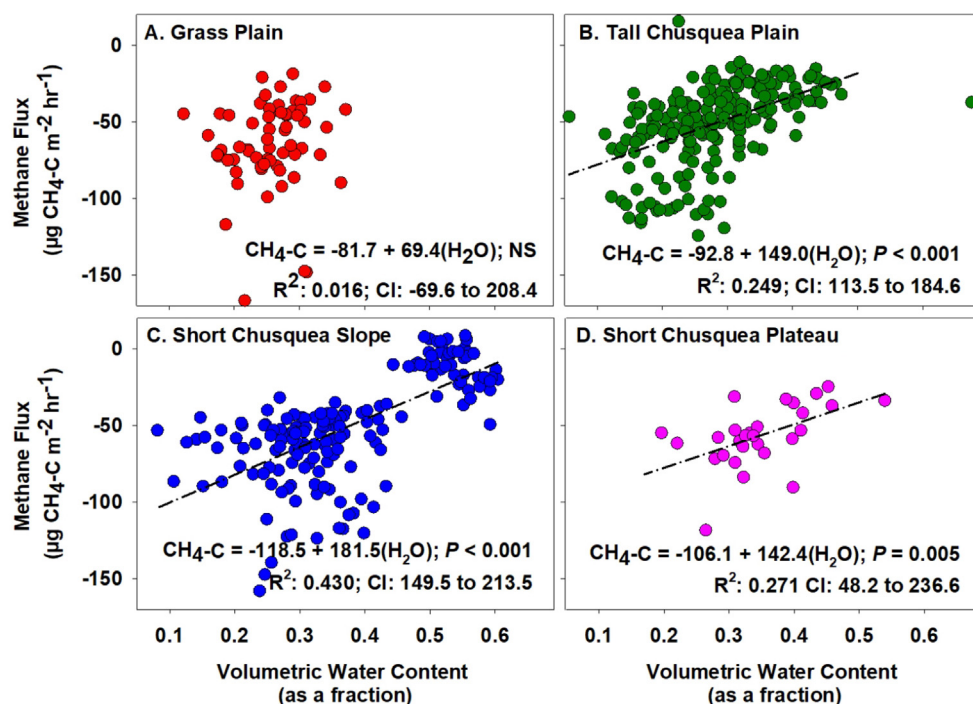
Fig. 6. Methane fluxes as a function of soil volumetric water content in the 0–6 cm surface soil layer when comparing the four terrain-vegetation sub-areas in our study site. The parameters derived from ordinary least square linear regressions as well as p-values and confidence intervals (alpha: 0.05) of the regression coefficient (slope) for each data subset are provided. NS stands for a non-significant slope; linear fitting was drawn only when slope was significant at alpha: 0.05. All panels use the same scales to enable visual comparison. The number of observations for each field sub-area are (panel A) grassy plain: 65, (B) tall *Chusquea* plain: 209, (C) short *Chusquea* slope: 170, and (D) short *Chusquea* plateau: 28.

other alpine environments (Table 2). These studies, including locations within the Tibetan Plateau, the Austrian Alps, Mt. Kilimanjaro, and the Rocky Mountains, measured methane uptake with magnitudes typically ranging from -66.2 to -0.52 µg CH_4-C m^{-2} hr^{-1}. Compared to this range of methane sinks, our results indicate a considerable methane uptake in the Central American páramo during the transient onset of a rainy period. Indeed, it is likely that the páramo is a methane sink during most of the dry season (December to April) too, as soil and weather conditions are comparable (Fig. 2 and Supplementary Fig. 1). To date, no other measurements of CH_4 flux in the neotropical páramo have been reported in the literature. Our study contributes to filling this knowledge gap and also points to the need for further flux research in these unique neotropical alpine ecosystems, including other components of the widely heterogeneous páramo landscape such as summits, higher slopes, wetlands, and alpine lakes, and also during the wet periods with increased rainfall (e.g., May to June, September to November; Supplementary Fig. 1A).

In our study site, the landscape area with the overall largest uptake of CH_4 was the grassy plain (Fig. 4A), and this pronounced uptake of CH_4 was stronger than in the tall *Chusquea* plain and the short *Chusquea* slope. The relatively higher uptake in the grassy plain than within the *Chusquea*-dominated terrains can be attributed to a combined effect of the differing topographic positions across the field and also their contrasting internal drainage. As shown by the soil profile characterization (Table 1), water drainage at the plateau and along the slope was imperfect. Moreover, our results of soil moisture at the surface layer further confirmed that the slope terrain dominated by short *Chusquea* was the wettest field sub-area (Fig. 4C). Collectively, this evidence revealed a distinctive, underlying soil gradient, with a sustained higher moisture at the slope and plateau areas, sharply declining with the transition into the tall *Chusquea* plain, and gradually decreasing even more into the drier, meadow plain dominated by grasses.

The gleyed Cg horizon underlying the slope and plateau areas was found to be heavily consolidated, creating a semi-impermeable layer that caused water perching and saturated conditions in these soil profiles for extended, recurrent periods. This pedogenic inference was supported by the noticeable incidence of prominent mottling features derived from redoximorphic processes within these soil profiles in the plateau and slope locations. By contrast, the soil profile at the lower terrain elevation in the grassy plain was underlain by a sandy subsurface layer and rocky glacial till, and this parent material layer was not heavily compacted. Based on the absence of pedogenic gleyization (Table 1), the glacial till parent material layer allowed free movement of water deeper and out of this soil profile. Differences in the permeability of these subsurface layers across the terrain gradient likely restricted downward water movement within in the plateau and slope profiles so that the upper soil horizons become wetter (Fig. 4C). However, as the glacial till layer becomes less consolidated in the grassy plain, the water is more free to penetrate rapidly and percolate deeper through the profile; therefore, the soil in this páramo plain dominated by native grass vegetation becomes better drained and aerated. In fact, the water table beneath this grassy plain may fluctuate deep enough that even *Chusquea* plants are not capable of accessing sufficient water to become established and to sustain *Chusquea* encroachment into the open meadows. These putative relationships require future investigation. Likewise, additional research is required to understand the causes of the apparent difference in overall methane uptake between the grassy plain and the tall *Chusquea* plain despite their corresponding soil moisture contents being mostly similar (Fig. 4).

In our study, soils with volumetric water contents ranging within 10 to 30% typically generated the more intense methane uptakes, while gradual increases in wetness decreased this CH_4 sink capacity (Fig. 5B). In fact, substantial soil CH_4 consumptions were only observed with water contents below 43% (Fig. 5A). As conceptually postulated by Dunfield (2007), a convex response curve can be ascertained for our methane fluxes as a function of moisture availability (Fig. 5B). These notions are in line with available reports. Chen et al. (2013) suggested slight enhancements in methane uptake in semiarid steppe soils experiencing intermediate water contents. Similarly, on a dry arctic site in West Greenland, D'Imperio et al. (2017) reported volumetric water content as the main controlling factor on CH_4 fluxes, as the highest CH_4 uptakes were associated with reduced soil moisture. Likewise, a study by Brachmann (2019) in a temperate alpine ecosystem documented enhanced methane uptake in midsummer (i.e., early August) when soil volumetric water content was below 26% mediated in part by alpine vegetation cover which collectively led to evident hot spots for intense
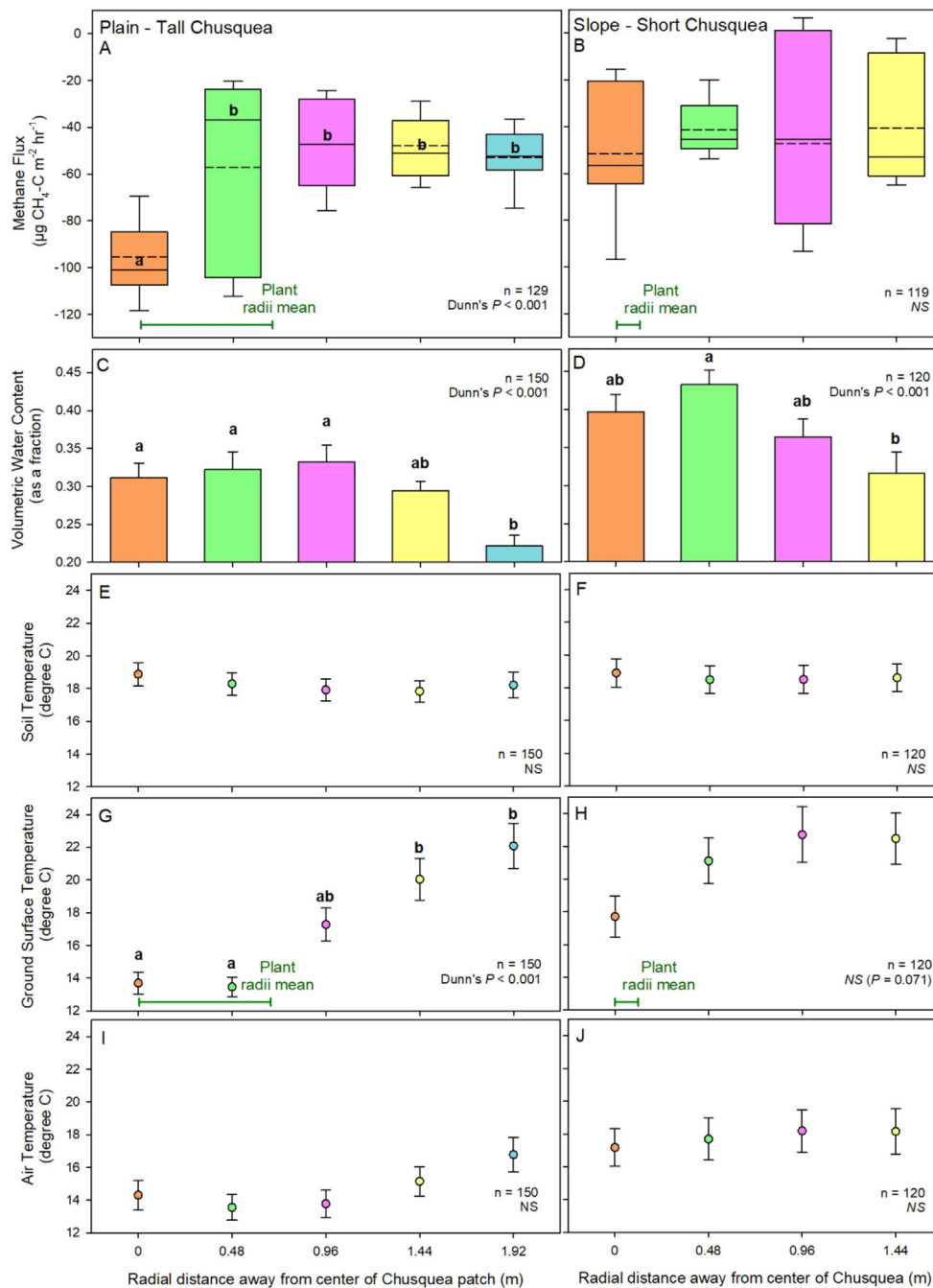
Fig. 7. (A, B) Methane fluxes, (C, D) soil volumetric water content and (E, F) soil temperature both in the 0–6 cm surface soil layer, (G, H) ground surface infrared temperature, and (I, J) air temperature within and near *Chusquea*. Data shown in left panels are for tall *Chusquea* patches in the plain sub-area, and right panels correspond to short *Chusquea* plants in the slope sub-area (see Fig. 1). Typical radii means of the *Chusquea* patches are indicated (further detailed in Site Description section). Lower case letters indicate the grouping comparison as based on Kruskal-Wallis followed by Dunn tests. Box plot representation in panels A and B: whiskers are the 10th and 90th percentiles, boundaries of the boxes are 25th and 75th percentiles, the continuous horizontal lines within the boxes are the medians, and discontinuous horizontal lines are the means. All panels showing temperature results (E, F, G, H, I, J) use the same scales to enable visual comparison. Error bars shown in panels C, D, E, F, G, H, I, J are standard errors.

CH_4 sink activity. Yet, we acknowledge that the maximum rates of CH_4 consumption likely occur at subsurface layers of the soil where moisture and temperature can be favorably stable, and that our topsoil moisture and temperature data served just as proxy indicators of these deeper soil conditions. Furthermore, as volumetric water content was effective in explaining the variations in CH_4 sink rates in the studied soils, future research could further incorporate water-filled pore space in conjunction with soil bulk density as a promising metric of water status (Meier et al., 2016; McKnight et al., 2017) for unraveling additional insights into moisture-aeration effects on soil CH_4 fluxes. Likewise, our findings of CH_4 sinks in the páramo could be further expanded by examining the magnitude of CH_4 fluxes during wetter periods which could hypothetically shift these alpine environments to becoming a methane source for part of the year, which has been observed for alpine wetlands (Chen et al., 2011; He et al., 2014; Teh et al., 2014).

As a proxy for the biological activity of soils and root respiration,

surface CO_2 fluxes were also found to be associated with soil moisture across the different vegetation types along our study site (Fig. 4B), but in a different way than the methane fluxes. In general, increases in moisture across the four field sub-areas triggered enlarged CO_2 emissions (Fig. 4B and C). In addition to this soil moisture stimulating effect, as expected, soil temperature exhibited an association with the individual CO_2 fluxes (Spearman's Rank correlation: 0.25; $P < 0.001$). Both moisture and heat availabilities are drivers of such biological activity (Hernandez-Ramirez et al., 2011; Curtin et al., 2012; McKnight et al., 2017; Sjogersten et al., 2018).

4.2. Overall vegetation effects on fluxes

The presence of distinct vegetation types along the studied toposequence in Valle de Los Conejos may also be contributing to differences in methane uptake. The noticeably denser root systems of *Chusquea*

Table 2

Compilation of methane fluxes from alpine ecosystems worldwide. Fluxes have been converted from the units in the original publications to µg CH_4-C m^{-2} hr^{-1}. When available, data ranges are shown within parentheses. Elevation expressed as meters above sea level (masl).

CH_4-C Flux (µg CH_4-C m^{-2} hr^{-1})	Site Characteristics and Location	Study Period	Country	References
−53.1 (−166.6 to 15.7, n: 472)	Valle de Los Conejos, Chirripó National Park, páramo, 3480 masl	10 samplings – 7 to 11 Apr. 2018	Costa Rica	This study
−50 (−141.7 to 0)	Colorado, Rocky Mountains, 2920 masl	11 samplings – springs and summers in 1991, 1992, and 1993	United States	Torn and Harte (1996)
−66.2	Bayinbuluk Grassland (alpine grassland), Tianshan Mountains, 2500 masl, sheep grazing	60 samplings – May 2010 to Oct. 2012	China	He et al. (2014)
−65.6 and −31.3 (2 years of data)	Tyrol, Eastern Alps, alpine dry meadow, 2250 masl	22 samplings – Oct. 2002 to Sep. 2004	Austria	Koch et al. (2007)
−53.6 (−71.85 to −36.6)	Alpine Steppe, Tibetan Plateau, 4730 masl, grazed and fenced meadow	105 samplings – May to Sep. each year from 2009 to 2013	China	Wei et al. (2015)
−44.4	Alpine meadow, Tibetan Plateau, 4900 masl, grazed and fenced meadow	42 samplings – May to Sep. each year from 2012 to 2013	China	Wei et al. (2015)
(−48.7 to −40.0)	Tianshan Mountains, China, 2500 masl, Alpine grassland	10 samplings – June 2010 to May 2011	China	Li et al. (2012)
(−53.9 to −1.05)	Alpine Meadow, sedges, grasses. Haibei Station, Tibetan Plateau, 3250 masl	21 samplings – May to Sep. 2007	China	Jiang et al. (2010)
−23.3	Qinghai-Tibetan Plateau, alpine meadow, grazed	42 samplings – May to Sep. 2008 and May to Sep. 2009	China	Fang et al. (2014)
(−34.3 to −3.7)	Mount Kilimanjaro, 3880 masl	24 samplings – 25 to 30 Nov. 2014	Tanzania	Guetlein et al. (2017)
−21.5	Alpine Meadow, Qinghai-Tibetan Plateau, > 4000 masl	1 sampling – 21 July 2005	China	Kato et al. (2011)
−99.0	Alpine Shrubland, Qinghai-Tibetan Plateau, > 4000 masl	1 sampling – 23 July 2005	China	Kato et al. (2011)
−0.52	Alp Weissenstein, Swiss Alps, 2000 masl, manure in fall.	17 samplings – June 2010 to June 2011	Switzerland	Imer et al. (2013)
650	Tres Cruces, Manu National Park, a grassland type referred to as "puna" (i.e., a wet Andean alpine ecosystem contrasting to the relatively less wet páramos), 3200–3700 masl	13 samplings – Dec. 2010 to Dec. 2011	Peru	Teh et al. (2014)

(Schneidt et al., 1996) compared to the grasses may contribute to soil aeration, increasing the transfers of oxygen and methane much deeper into a well-structured soil (Meier et al., 2016). Tanthachoon et al. (2008) showed that plants with longer and wider root systems were able to facilitate the supply of oxygen within the soil profile as well as support the presence of methanotrophs deeper in the soil, thus enhancing methane uptake and oxidation. Furthermore, based on their observations of larger aboveground biomass, Tol and Cleef (1994) suggested a greater belowground biomass and stronger root system for *Chusquea tessellata* as compared to typical Andean páramo grasses. Although it can be presumed that *Chusquea* growth favors soil structure formation, our study showed that drainage-impeding subsurface layers leading to poor aeration of the soil profile (as observed in the slope and plateau profile locations) can counteract and in certain extreme cases even fully negate these potential vegetation effects of enlarging the methane sink.

4.3. Chusquea patches and their fluxes

When delineating the four vegetation types in our field site (Fig. 1B), we noted that the size and abundance of *Chusquea* plants changed abruptly from a plain area where tall *Chusquea* grew in well-defined patches (and with wider natural openings in between these clumps) to the slope and plateau areas, where short *Chusquea* plants were more scattered. These visually evident divergences in morphological and spatial distribution of *Chusquea* vegetation across our field site are likely a combined effect of the underlying topographic and drainage attributes. As discussed above, the slope and plateau soils were observed to be imperfectly drained, while the plain soil was relatively drier and had a deep effective drainage. The higher soil moisture found in the slope and plateau (Fig. 4A) can increase growth and competition by other plant species (e.g., the grass *F. dolichophylla*) hindering *Chusquea*, whereas in certain field microsites of the relatively drier plains, *Chusquea* patches with putatively denser roots can develop and expand tall, vigorous canopies as they might access sufficient water within the profile.

As aforementioned, we evaluated replicated short-distance transects established radially from the center of the *Chusquea* plants with the aim of examining the responses of CH_4 fluxes to the two observed *Chusquea* phenotypes (tall-clumped vs. short *Chusquea*) (Figs. 1B and 3). This approach enabled comparing both between and within these *Chusquea* vegetation types as well as relative to their surrounding grass vegetation. Our flux results within the tall *Chusquea* plain revealed that the centers of these tall *Chusquea* patches had double the methane uptake rate as compared to the soils immediately outside these patches (Fig. 7A; Supplementary Fig. 3), and this clear effect was not caused by the short *Chusquea* plants growing in the slope sub-area (Fig. 7B). These localized, hot-spots for strong CH_4 sinks only-occurred beneath the tall *Chusquea* and appear to be intrinsically created by the presence of this vigorous vegetation, likely as an effect of their dense root system (Schneidt et al., 1996) generating suitable conditions for soil methanotrophy, as associated with efficient gas diffusion and exchange. This tall *Chusquea* effect was observed even when the soil beneath tall *Chusquea* patches was wetter than under the surrounding grass vegetation (Fig. 7C). Indeed, these tall *Chusquea* patches in the páramo plains override and even exceedingly offset the effect of soil moisture on CH_4 flux as discussed above (Figs. 5 and 7). Moreover, as *Chusquea* height was associated with the intensity of CH_4 uptake, future research can undertake remote sensing approaches for examining vegetation attributes (e.g., leaf area index, photosynthetic rate, canopy heat stress, height, biomass) as potential proxies to estimate CH_4 uptake and with the goal of subsequently developing flux mapping at the landscape scale.

Results from an earlier study by Chen et al. (2011) in a temperate alpine wetland suggest that distinct vegetation types can be associated with contrasting field microsites that widely shift the magnitude of the

net CH_4 flux, and even change the flux direction between uptake and emission. Likewise, Hofmann et al. (2016) also documented contrasting CH_4 fluxes depending on vegetation types such as forest and grassland in temperate montane and subalpine sites. Our findings in the neotropical páramo further support these relationships. Based on these observations, it becomes plausible that tall *Chusquea* vegetation in páramo plains facilitates the uptake of atmospheric methane consistently throughout the year, and even during the wetter periods of rainy seasons. This hypothesis warrants future investigation of the *Chusquea* effect on methane fluxes. Tall *Chusquea*'s dense canopy, shade and litter layer can provide a more favorable, stable microclimate, preventing excessive desiccation and any crusting or sealing at the soil surface, which collectively enhanced and sustained methane uptake and likely overall biological activity. These presumptions are supported by the distinctively cooler, moist conditions found under the canopy of tall *Chusquea* vegetation (Fig. 7G and C) in the same locations where methane uptake was much enhanced (Fig. 7A).

5. Conclusion

One of the key drivers of CH_4 fluxes in the páramo was soil moisture, which was ultimately regulated by spatial variations in vegetation, topography and soil profile drainage attributes. Our study depicted a gradient of soils and vegetation, revealing that sites without drainage-impeding soil layers or with the facilitating presence of vigorous *Chusquea* vegetation lead to relatively stronger sinks of methane as compared to fields with wetter, less aerated soils.

To our knowledge, this is the first study to quantify methane fluxes in a neotropical páramo ecosystem, suggesting that these alpine landscapes act in general as a substantial sink of atmospheric CH_4. These flux data offer a detailed snapshot in time and space of the methane uptake rates in a Central American páramo in the beginning of the rainy season which is a critical period of intense biophysical and biogeochemical shifts in this ecosystem. Future research can examine how CH_4 fluxes in these alpine landscapes respond during the torrential rainy season, and their potential switch into CH_4 sources when soils become excessively wet. It is also uncertain how the net CH_4 exchange will respond in these ecosystems to increased intensification of climatic variability and extent of droughts as projected for the Central American páramo.

Declaration of Competing Interest

The authors declare that they have no known competing financial interests or personal relationships that could have appeared to influence the work reported in this paper.

Appendix A. Supplementary data

Supplementary data to this article can be found online at https://doi.org/10.1016/j.geoderma.2019.114092.

References

Beniston, M., 2000. Environmental Change in Mountains and Uplands. Arnold Publishers, New York.

Brachmann, C.G., 2019. Characteristics of alpine plants and soils along an elevational gradient, Northern Selkirk Mountains, British Columbia. Master of Science thesis, Department of Biological Sciences, University of Alberta. 130 p.

Buytaert, W., Célleri, R., De Bievre, D.B., Cisneros, F., Wyseure, G., Deckers, J., Hofstede, R., 2006a. Human impact on the hydrology of the Andean Páramos. Earth Sci. Rev. 79, 53–72. https://doi.org/10.1016/j.earscirev.2006.06.002.

Buytaert, W., Deckers, J., Wyseure, G., 2006b. Description and classification of non-allophanic Andosols in south Ecuadorian alpine grasslands (páramo). Geomorphology 73 (3–4), 207–221. https://doi.org/10.1016/j.geomorph.2005.06.012.

Célleri, R., Buytaert, W., De Bièvre, B., Tobón, C., Crespo, P., Molina, J., Feyen, J., 2010. Understanding the Hydrology of Tropical Andean Ecosystems Through an Andean Network of Basins. Status and Perspectives of Hydrology in Small Basins. IAHS Publication, Goslar-Hahnenklee, Germany.

Chen, H., Wu, N., Wang, Y., Gao, Y., Peng, C., 2011. Methane fluxes from alpine wetlands of Zoige Plateau in relation to water regime and vegetation under two scales. Water Air Soil Pollut. 217, 173–183. https://doi.org/10.1007/s11270-010-0577-8.

Chen, W., Zheng, X., Chen, Q., Wolf, B., Butterbach-Bahl, K., Brüggemann, N., Lin, S., 2013. Effects of increasing precipitation and nitrogen deposition on CH_4 and N_2O fluxes and ecosystem respiration in a degraded steppe in Inner Mongolia, China. Geoderma 192, 335–340. https://doi.org/10.1016/j.geoderma.2012.08.018.

Curtin, D., Beare, M.H., Hernandez-Ramirez, G., 2012. Temperature and moisture effects on microbial biomass and soil organic matter mineralization. Soil Sci. Soc. Am. J. 76, 2055–2067. https://doi.org/10.2136/sssaj2012.0011.

D'Imperio, L., Nielsen, C.S., Westergaard-Nielsen, A., Michelsen, A., Elberling, B., 2017. Methane oxidation in contrasting soil types: responses to experimental warming with implication for landscape-integrated CH_4 budget. Glob. Chang. Biol. 23, 966–976. https://doi.org/10.1111/gcb.13400.

Dunfield, P.F., 2007. The soil methane sink. In: Reay, D.S., Hewitt, C.N., Smith, K.A., Grace, J. (Eds.), Greenhouse Gas Sinks. CAB International, Wallingford, UK, pp. 152–157.

Durán-Quesada, A.M., Gimeno, L., Amador, J.A., 2017. Role of moisture transport for Central American precipitation. Earth Syst. Dynam. 8, 147–161. https://doi.org/10.5194/esd-8-147-2017.

Esquivel-Hernández, G., Mosquera, G.M., Sánchez-Murillo, R., Quesada-Román, A., Birkel, C., Crespo, P., Célleri, R., Windhorst, D., Breuer, L., Boll, J., 2019. Moisture transport and seasonal variations in the stable isotopic composition of rainfall in Central American and Andean Páramo during El Niño conditions (2015–2016). Hydrol. Process. 33 (13), 1802–1817. https://doi.org/10.1002/hyp.13438.

Esquivel-Hernández, G., Sánchez-Murillo, R., Quesada-Román, A., Mosquera, G., Birkel, C., Boll, J., 2018. Insight into the stable isotopic composition of glacial lakes in a tropical alpine ecosystem: Chirripó, Costa Rica. Hydrol. Process. 32 (24), 3588–3603. https://doi.org/10.1002/hyp.13286.

Fang, H., Cheng, S., Yu, G., Cooch, J., Wang, Y., Xu, M., Li, L., Dang, X., Li, Y., 2014. Low-level nitrogen deposition significantly inhibits methane uptake from an alpine meadow soil on the Qinghai-Tibetan Plateau. Geoderma 213, 444–452. https://doi.org/10.1016/j.geoderma.2013.08.006.

Girkin, N.T., Vane, C.H., Cooper, H.V., Moss-Hayes, V., Craigon, J., Turner, B.L., Ostle, N., Sjogersten, S., 2019. Spatial variability of organic matter properties determines methane fluxes in a tropical forested peatland. Biogeochemistry 142, 231–245. https://doi.org/10.1007/s10533-018-0531-1.

Guetlein, A., Zistl-Schlingmann, M., Becker, J.N., Cornejo, N.S., Detsch, F., Dannenmann, M., Appelhans, T., Hertel, D., Kuzyakov, Y., Kiese, R., 2017. Nitrogen turnover and greenhouse gas emissions in a tropical alpine ecosystem, Mt. Kilimanjaro, Tanzania. Plant Soil 411, 243–259. https://doi.org/10.1007/s11104-016-3029-4.

He, G., Li, K., Liu, X., Gong, Y., Hu, Y., 2014. Fluxes of methane, carbon dioxide and nitrous oxide in an alpine wetland and an alpine grassland of the Tianshan Mountains, China. J. Arid Land. 6, 717–724. https://doi.org/10.1007/s40333-014-0070-0.

Hernandez-Ramirez, G., Hatfield, J.L., Parkin, T.B., Sauer, T.J., Prueger, J.H., 2011. Carbon dioxide fluxes in corn-soybean rotations in the Midwestern U.S.: inter- and intra-annual variations, and biophysical controls. Agric. Forest. Meteor. 151, 1831–1842. https://doi.org/10.1016/j.agrformet.2011.07.017.

Hofmann, K., Farbmacher, S., Illmer, P., 2016. Methane flux in montane and subalpine soils of the Central and Northern Alps. Geoderma 281, 83–89. https://doi.org/10.1016/j.geoderma.2016.06.030.

Hofstede, R., Segarra, P., Mena, P., 2003. Los Páramos del Mundo: Proyecto Atlas Mundial de los Páramos. Global Peatland Initiative/NC/IUCN/EcoCiencia, Quito, Ecuador.

Imer, D., Merbold, L., Eugster, W., Buchmann, N., 2013. Temporal and spatial variations of soil CO_2, CH_4 and N_2O fluxes at three differently managed grasslands. Biogeosciences 10, 5931–5945. https://doi.org/10.5194/bg-10-5931-2013.

Jang, I., Lee, S., Hong, J., Kang, H., 2006. Methane oxidation rates in forest soils and their controlling variables: a review and a case study in Korea. Ecol. Res. 21 (6), 849–854. https://doi.org/10.1007/s11284-006-0041-9.

Jiang, C., Yu, G., Fang, H., Cao, G., Li, Y., 2010. Short-term effect of increasing nitrogen deposition on CO_2, CH_4 and N_2O fluxes in an alpine meadow on the Qinghai-Tibetan Plateau, China. Atmos. Environ. 44 (24), 2920–2926. https://doi.org/10.1016/j.atmosenv.2010.03.030.

Kappelle, M., Horn, S.P., 2016. The Páramo ecosystem of Costa Rica's highlands. In: Kappelle, M. (Ed.), Costa Rican Ecosystems. University of Chicago Press, Chicago, pp. 492–523.

Kato, T., Hirota, M., Tang, Y., Wada, E., 2011. Spatial variability of CH_4 and N_2O fluxes in alpine ecosystems on the Qinghai-Tibetan Plateau. Atmos Environ. 45 (31), 5632–5639. https://doi.org/10.1016/j.atmosenv.2011.03.010.

Kim, D.G., Giltrap, D., Hernandez-Ramirez, G., 2013. Background nitrous oxide emissions in agricultural and natural lands: a meta-analysis. Plant Soil 373, 17–30. https://doi.org/10.1007/s11104-013-1762-5.

Koch, O., Tscherko, D., Kandeler, E., 2007. Seasonal and diurnal net methane emissions from organic soils of the Eastern Alps, Austria: effects of soil temperature, water balance, and plant biomass. Arct. Antarct. Alp. Res. 39 (3), 438–448. https://doi.org/10.1657/1523-0430(06-020)[KOCH]2.0.CO;2.

Kou, Y., Li, J., Wang, Y., Li, C., Tu, B., Yao, M., Li, X., 2017. Scale-dependent key drivers controlling methane oxidation potential in Chinese grassland soils. Soil Biol. Biochem. 111, 104–114. https://doi.org/10.1016/j.soilbio.2017.04.005.

Li, K., Gong, Y., Song, W., He, G., Hu, Y., Tian, C., Liu, X., 2012. Responses of CH_4, CO_2 and N_2O fluxes to increasing nitrogen deposition in alpine grassland of the Tianshan Mountains. Chemosphere 88 (1), 140–143. https://doi.org/10.1016/j.chemosphere.2012.02.077.

Lin, S., Hernandez-Ramirez, G., Kryzanowski, L., Wallace, T., Grant, R., Degenhardt, R., Berger, N., Sprout, C., Lohstraeter, G., Powers, L.-A., 2017. Timing of manure injection and nitrification inhibitors impacts on nitrous oxide emissions and nitrogen transformations in a barley crop. Soil Sci. Soc. Am. J. 81, 1595–1605. https://doi.org/10.2136/sssaj2017.03.0093.

Magaña, V., Amador, J.A., Medina, S., 1999. The midsummer drought over Mexico and Central America. J. Clim. 12, 1577–1588. https://doi.org/10.1175/1520-0442(1999)012<1577:TMDOMA>2.0.CO;2.

McKnight, J.Y., Harden, C.P., Schaeffer, S.M., 2017. Soil CO_2 flux trends with differences in soil moisture among four types of land use in an Ecuadorian páramo landscape. Phys. Geog. 38, 51–61. https://doi.org/10.1080/02723646.2016.1256101.

Meier, I.C., Leuschner, C., Marini, E., Fender, A.-C., 2016. Species-specific effects of temperate trees on greenhouse gas exchange of forest soil are diminished by drought. Soil Biol. Biochem. 95, 122–134. https://doi.org/10.1016/j.soilbio.2015.12.005.

Orvis, K.H., Horn, S.P., 2000. Quaternary glaciers and climate on Cerro Chirripó, Costa Rica. Quat. Res. 54, 24–37. https://doi.org/10.1006/qres.2000.2142.

Schneidt, J., Stein, U., Furchheim-Weberling, B., Wiedmann, S., Weberling, F., 1996. Estudios sobre formas de crecimiento de algunas especies típicas del páramo de Costa Rica. Brenesia 45–46, 51–112.

Serrano-Silva, N., Sarria-Guzman, Y., Dendooven, L., Luna-Guido, M., 2014. Methanogenesis and methanotrophy in soil: A review. Pedosphere 24 (3), 291–307. https://doi.org/10.1016/S1002-0160(14)60016-3.

Sjogersten, S., Aplin, P., Gauci, V., Peacock, M., Siegenthaler, A., Turner, B.L., 2018. Temperature response of ex-situ greenhouse gas emissions from tropical peatlands: Interactions between forest type and peat moisture conditions. Geoderma 324, 47–55. https://doi.org/10.1016/j.geoderma.2018.02.029.

Soil Classification Working Group 1998. The Canadian System of Soil Classification. Haynes, R.H., OC, and FRSC (Eds.). third ed. Ottawa, NRC Monograph Publishing Program.

Tanthachoon, N., Chiemchaisri, C., Chlemchaisri, W., Tudsri, S., Kumar, S., 2008. Methane oxidation in compost-based landfill cover with vegetation during wet and dry conditions in the tropics. J Air Waste Manage. Assoc. 58 (5), 603–612. https://doi.org/10.3155/1047-3289.58.5.603.

Teh, Y.A., Diem, T., Jones, S., Huaraca Quispe, L.P., Baggs, E., Morley, N., Richards, M., Smith, P., Meir, P., 2014. Methane and nitrous oxide fluxes across an elevation gradient in the tropical Peruvian Andes. Biogeosciences 11, 2325–2339. https://doi.org/10.5194/bg-11-2325-2014.

Tol, G.J., Cleef, A.M., 1994. Above ground biomass structure of a *Chusquea tessellata* bamboo Páramo, Chingaza National Park, Cordillera Oriental, Colombia. Vegetatio 115, 29–39. https://doi.org/10.1007/BF00119384.

Torn, M.S., Harte, J., 1996. Methane consumption by montane soils: implications for positive and negative feedback with climatic change. Biogeochemistry 32 (1), 53–67. https://doi.org/10.1007/BF00001532.

Wei, D., Xu, R., Tenzin, T., Wang, Y., Wang, Y., 2015. Considerable methane uptake by alpine grasslands despite the cold climate: in situ measurements on the central Tibetan Plateau, 2008–2013. Glob. Chang. Biol. 21 (2), 777–788. https://doi.org/10.1111/gcb.12690.